Analytical Methods

RSC Publishing

PAPER

View Article Online
View Journal | View Issue

Cite this: *Anal. Methods*, 2013, **5**, 6611

Imaging cellular uptake and intracellular distribution of TiO_2 nanoparticles†

Jichao Zhang,[ab] Xiaoqing Cai,*[a] Yi Zhang,[a] Xiaoming Li,[a] Wenxin Li,[a] Yangchao Tian,[c] Aiguo Li,[b] Xiaohan Yu,[b] Chunhai Fan[a] and Qing Huang*[a]

Received 8th July 2013
Accepted 9th September 2013

DOI: 10.1039/c3ay41121d

www.rsc.org/methods

Understanding the internalization of nanoparticles in cells is of great interest for diagnostic and therapeutic applications. We investigated the cellular uptake and distribution of TiO_2 nanoparticles by high lateral resolution transmission electron microscopy (TEM) and transmission X-ray microscopy. TEM results showed that TiO_2 nanoparticle internalization mostly occurred *via* endocytosis and the nanoparticles were distributed in the cytoplasm. 3D reconstructed tomography also confirmed that TiO_2 nanoparticle aggregates were mainly distributed over the cell membrane surface.

Introduction

Nanoscale materials (particle size <100 nm) are of great interest because of their unique optical, electrical, and magnetic properties. Their specific properties, such as small size, shape and high surface area, make them promising candidates for industrial and biomedical applications.[1–3] As fine particles, normal-sized (>100 nm) TiO_2 is considered to be biologically inert toward animals and humans,[4] and it is widely used as an ingredient in paints, and as an additive in food colouring and cosmetic products. TiO_2 nanoparticles (1–100 nm) are typical metal oxide nanomaterials and are also "manufactured nanoparticles" that are widely used in the biomedical field because of their photocatalytic activity and UV light absorption properties.[5]

Recent studies into the toxicity of TiO_2 nanoparticles have increased dramatically, and many more are in progress. Investigations into the cytotoxicity of TiO_2 nanoparticles are not always consistent and contradictory reports on the cytotoxicity of TiO_2 nanoparticles exist. Zhang and Sun found that 90% of human colon carcinoma cells survived even after 24 h of exposure to 1000 μg ml^{-1} TiO_2 nanoparticles.[6] Nakagawa *et al.* reported no effect of ultra-fine (25 nm) TiO_2 on a series of genotoxicity parameters.[7] Conversely, Rahman *et al.* found that exposure of Syrian hamster embryo cells (SHE) to 1 μg cm^{-2} TiO_2 nanoparticles for 12–72 h caused a significant dose-dependent increase in the induction of cell apoptosis.[8] Wang *et al.* also found that TiO_2 nanoparticles are cytotoxic (MTT assay), genotoxic (Comet and cytokinesis block micronucleus (CBMN) assays) and mutagenic (HPRT mutation assay) towards cultured WIL2-NS human lymphoblastoid cells.[9] Jin *et al.* found that TiO_2 nanoparticles could induce significant cytotoxicity in L929 cells. Cell adhesion, proliferation *via* lysosome enhancement, oxidative stress and DNA damage were affected by the presence of TiO_2 nanoparticles in a dose-dependent manner.[10] Gurr *et al.* reported that anatase TiO_2 nanoparticles (10 and 20 nm) induced an increase of intracellular reactive oxygen species (ROS), malondialdehyde (MDA) levels, and DNA oxidation in BEAS-2B cells in the absence of photoactivation.[11]

To investigate these contradictory experimental results, the determination of cellular uptake and the distribution of TiO_2 nanoparticles are critical. Some reports exist about the animal distribution of TiO_2 nanoparticles,[12–15] but to date the cellular uptake and distribution of TiO_2 nanoparticles are still not clear. The biggest obstacle is imaging technique restrictions. The cellular uptake and distribution of nanomaterials are commonly investigated by optical microscopy and transmission electron microscopy (TEM). Optical microscopy and confocal microscopy have low spatial resolution (usually much larger than 200 nm), and fluorescent labeling in the confocal microscope cannot easily provide unique three-dimensional (3D) structural information about whole cells. TEM can provide important two-dimensional (2D) structural information because of its high spatial resolution. However, it is difficult to obtain 3D images of cells. Thus, new high-throughput high-resolution imaging techniques are imperative for such extensive investigations.[16] X-ray microscopy can be divided into soft X-ray microscopy and hard X-ray microscopy according to the photon energy range used. Soft X-ray microscopy gives natural contrast

[a]*Laboratory of Physical Biology and Shanghai Synchrotron Radiation Facility, Shanghai Institute of Applied Physics, Chinese Academy of Sciences, Shanghai 201800, People's Republic of China. E-mail: caixiaoqing@sinap.ac.cn; huangqing@sinap.ac.cn; Tel: +86-21-39194068; +86-21-39194520*

[b]*Shanghai Synchrotron Radiation Facility, Shanghai Institute of Applied Physics, Chinese Academy of Sciences, Shanghai 201800, People's Republic of China. E-mail: caixiaoqing@sinap.ac.cn; huangqing@sinap.ac.cn; Tel: +86-21-39194068; +86-21-39194520*

[c]*National Synchrotron Radiation Laboratory, University of Science and Technology of China, Hefei, Anhui, 230029, People's Republic of China*

† Electronic supplementary information (ESI) available. See DOI: 10.1039/c3ay41121d

between organic materials and water using wavelengths in the range of the "water-window". The cellular structures of whole, hydrated cells can be imaged without staining.[17,18] The resolution is dozens of nanometers and the penetration range can be up to 10 μm for a fully hydrated sample.[19,20] However, because of the small depth of focus and the weak penetration power of soft X-rays, soft X-ray microscopy is incapable of imaging many eukaryotic cells, especially when tomography imaging is needed.

Full-field hard X-ray microscopy is another fascinating complementary imaging method with a large depth of focus because of its high penetration power. Compared with soft X-ray imaging, hard X-ray microscopy has the potential to image cells up to several tens of micrometers. Progress in the field of X-ray optics allows the resolution of full-field hard X-ray microscopy to be 20–50 nm in many facilities.[21–25] Tomography is a general tool used to obtain 3D information in diagnostic medical imaging and a similar technology is now being used in TEM investigations. Remarkable 3D views of selected specimens can be generated including microorganisms and sections of cells,[26–28] However, this technology can reveal extraordinary details. The preparation processes are time-consuming and involve embedding and other steps that can lead to artifacts. Transmission X-ray microscopy (TXM) is another method to generate 3D information from whole cells and it is widely used to produce high-resolution images for the examination of whole, hydrated cells.[29–34] It has been demonstrated to be an effective imaging method for the study of nanoparticle distributions at the subcellular level, providing sufficient lateral resolution to image internalized particles.[29–31] Highly penetrating X-rays can be used to examine thick samples and tomographic reconstructions can reveal 3D localization, which is particularly useful for the analysis of nanoparticles within single cells.[35–37]

We used high lateral resolution transmission electron microscopy (HRTEM) and TXM to investigate cellular uptake and distribution imaging of TiO_2 nanoparticles in Human cervical cancer (HeLa) cells. TEM results show that TiO_2 nanoparticle internalization mostly occurred *via* endocytosis and the nanoparticles are distributed in the cytoplasm. TXM provided additional information about the cellular surface distribution of TiO_2 nanoparticle aggregates and changes in the HeLa cell morphology. This information cannot be obtained by cytotoxicity MTT assays. These results are helpful in understanding the cellular uptake and distribution of TiO_2 nanoparticles, and are also helpful in extending the biological applications of X-ray microscopy. This technique's unique ability to image nanoparticle aggregate distribution in cells in 3D could see it become a complementary tool in cell imaging and thus provide useful information in cell biology.

Materials and methods

Materials

20 nm TiO_2 primary particles were purchased from Shanghai Hujing Sub-Nanoscale New Material Co. Ltd., Shanghai, China. High-sugar Dulbecco's modified Eagle's medium (DMEM) and fetal bovine serum (FBS) were purchased from Invitrogen (Paisley, UK). Human cervical cancer cells (HeLa cells) were purchased from Shanghai Cell Bank (Shanghai, China). 3-(4,5-Dimethylthiazol-2-yl)-2,5-diphenyltetrazolium bromide (MTT) and other chemical reagents were purchased from Sigma-Aldrich (St. Louis, USA).

Characterization of TiO_2 nanoparticles by TEM and DLS

The TiO_2 nanoparticle colloid was dispersed in deionized water, phosphate buffered saline (PBS) or culture medium with or without FBS. After ultrasonication for 5 min, the TiO_2 nanoparticle colloid solutions were analyzed by transmission electron microscopy (TEM, JEM2010F, JEOL, Tokyo, Japan) and dynamic light scattering (DLS, ZETASIZER 3000HSA, Malvern Instruments Ltd., Worcestershire, UK).

Cell culture and treatments

Human cervical cancer cells (HeLa cells) were cultured in Dulbecco's modified Eagle's medium (DMEM), and supplemented with 10% FBS, 100 U ml^{-1} penicillin and 100 μg ml^{-1} streptomycin at 37 °C in a humidified atmosphere composed of 5% CO_2. The cells were sub-cultured every 2–3 days. Subconfluent cultures were exposed to TiO_2 nanoparticles, formulated at 2 mg ml^{-1}, and added to the culture medium to a final concentration of 100 μg ml^{-1}.

Analysis of cell viability

Cell viability was measured using the 3-(4,5-dimethylthiazol-2-yl)-2,5-diphenyltetrazolium bromide (MTT) assay, which is based on the conversion of MTT to formazan by mitochondrial and cytosol dehydrogenases.[31,32] The cells were dispensed into 96-well plates over different incubation times. 10 μL stock MTT (5 mg ml^{-1}) was added to each well, and cells were then incubated for 4 h at 37 °C. The cells were lysed with sodium dodecyl sulfate (SDS). Absorbance was measured at 570 nm using a microplate reader (Bio-Rad 680, USA). All measurements were done in triplicate, and at least three independent experiments were carried out.

ICP-MS analysis of the TiO_2 content of HeLa cells

HeLa cells were exposed to 100 μg ml^{-1} TiO_2 nanoparticles over different time periods (0, 6, 12, 24, and 48 hours). The culture medium was removed and washed with PBS three times, and the cells were digested with trypsin solution for 10 min. Sonication was carried out for 2 h in a hot water bath to completely disrupt the cell membranes. Finally, the TiO_2 nanoparticles were dissolved by successively adding 0.4 ml aqua regia (the volume ratio of 37% HCl and 70% HNO_3 was 3 : 1). The solution was diluted with deionized water until the HCl concentration reached 2% (v). The TiO_2 contents were determined by inductively coupled plasma mass spectrometry (ICP-MS) (X7, Thermo Fisher, USA).

Transmission electron microscopy

HeLa cells were fixed with 2.5% glutaraldehyde in 0.1 M PBS and washed. After postfixation in 1% OsO_4 in PBS for 1 h, the

cells were dehydrated in a graded series of ethanol, treated with propylene oxide and embedded in Epon. Approximately 60–70 nm thick sections were cut using an LKB-Ultrotome V and transferred to Formvar-coated copper grids. The sections were stained with uranyl acetate and Reynolds lead citrate and examined on a Joel JEM-1230 transmission electron microscope at 80 kV at the Institute of Neuroscience Electron Microscopy Core (Shanghai, China).

X-ray microscopy analysis

TXM was performed on the X-ray microscope beamline U7A at the National Synchroton Radiation Laboratory (NSRL), Hefei, China. Cells were fixed with 2.5% glutaraldehyde in 0.1 M PBS and washed. The cells were dehydrated using a graded ethanol series (30%, 50%, 70%, 90% and 100%), each for 30 min. The cell suspension in 100% ethanol was dropped onto 100 nm thick silicon nitride support films. The samples were moved onto a silicon nitride window. Gold particles of 500–800 nm in size were used as alignment reference markers. Transmitted and scanning images were acquired by TXM. The absorption contrast imaging at 8 keV can be carried out using this microscopy system. To obtain 3D tomographical reconstructed images, raw images were collected at different angles from −75° to +75° with angle intervals of 1°. The 3D reconstruction was processed using Xradia software and displayed with Amira.

Results and discussion

Characterization of TiO_2 nanoparticles

The TiO_2 nanoparticles in aqueous solutions were examined by TEM and DLS. The TEM investigation indicated that the primary size of the TiO_2 nanoparticles is about 20 nm and this is consistent with the information supplied by the manufacturer. DLS was used to measure the mean distribution of TiO_2 nanoparticles diameter in DI water, PBS and culture medium with or without FBS. The primary size of TiO_2 nanoparticles is about 20 nm (Fig. 1A), but the aggregate size of the TiO_2 nanoparticles in DI water, PBS, culture medium without FBS and culture medium with FBS changed to 135.3 ± 1.6 nm, 309.3 ± 3.6 nm, 169.7 ± 1.9 nm and 68.6 ± 2.3 nm, respectively (Fig. 1B). These results show that TiO_2 nanoparticles are easily dispersed in cell culture medium with FBS (68.6 ± 2.3 nm) and are suitable for further cell experiments.

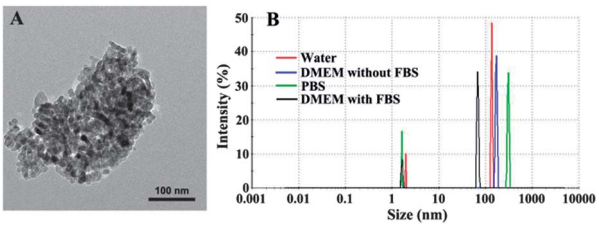

Fig. 1 TiO_2 nanoparticle size was characterized by (A) TEM and (B) DLS. (A) TEM image of TiO_2 nanoparticles (bar, 100 nm). (B) Aggregate sizes of TiO_2 nanoparticles in four solutions: water, 135.3 ± 1.6 nm; PBS, 309.3 ± 3.6 nm; DMEM without FBS, 169.7 ± 1.9 nm; DMEM with FBS, 68.6 ± 2.3 nm.

Effects on cell viability

The cell viability of the different concentrations of TiO_2 nanoparticles was evaluated by the MTT assay. HeLa cells were cultured in media containing TiO_2 nanoparticles for 6, 24 and 48 hours. As the concentration of TiO_2 nanoparticles increased (from 0 to 800 μg ml^{-1}) in the culture medium, the viability of the cells cultured for 6 and 24 h was not significantly altered (only 22% decrease in cell viability at 800 μg ml^{-1} over 24 h). However, significant cytotoxicity was observed after 48 h of cell culture at a high concentration. When compared with the control group, the cells cultured in medium containing 800 μg ml^{-1} TiO_2 nanoparticles for 48 h only exhibited a 42% decrease in viability (Fig. 2). The results show that TiO_2 nanoparticle concentrations did not have a marked effect on cell growth although there was a significant decrease over a long incubation time of 48 h.

Uptake and intracellular distribution of TiO_2 nanoparticles in HeLa cells

Nanoparticle internalization within cells is a potentially important factor in biological effects and in the enhancement of therapeutic effects. Cellular uptake was quantitatively investigated by ICP-MS. As shown in Fig. 3, the TiO_2 uptake by HeLa cells rapidly increased up to 6 h but then increased slowly over longer incubation times (24 h or 48 h). The total uptake of TiO_2 in cells depends on TiO_2 nanoparticle exposure times. These quantitative results demonstrate that TiO_2 nanoparticles are easily internalized by HeLa cells and uptake gradually increases depending on the incubation time.

Nanoparticles internalized in cells are generally believed to remain in endosomes because of endocytosis.[38] As shown in Fig. 4A, normal HeLa cells have very clear subcellular structures such as a cell nucleus (N) and mitochondria (M). Caveolae are the major non-clathrin-dependent route from the cell surface to the endosomes.[39] In our TEM study, many TiO_2 nanoparticles were present in the caveolae-like structure (Fig. 4B). For example, in Fig. 4C, TiO_2 nanoparticles were found in

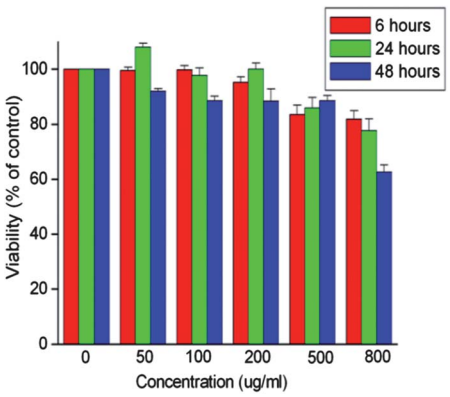

Fig. 2 Cytotoxicity of TiO_2 nanoparticles at different concentrations and incubation times toward HeLa cells. Cell viability was measured using the MTT assay (6, 24 and 48 h) and calculated as a percentage from the viability of the control (untreated) cells. The viability of the control cells was considered to be 100%. The results are mean ± SD from three independent experiments.

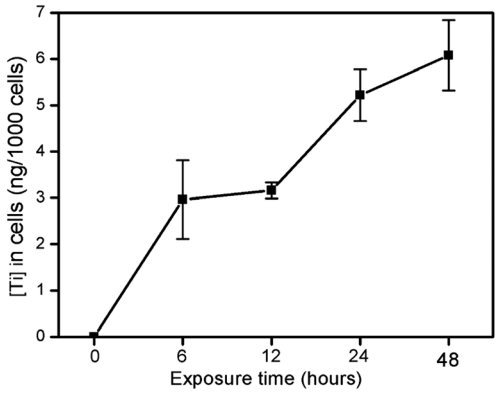

Fig. 3 Time dependence of Ti uptake in HeLa cells. HeLa cells were exposed to 100 μg ml^{-1} TiO_2 nanoparticles for 0 to 48 h, and the TiO_2 content in the cells was measured by ICP-MS.

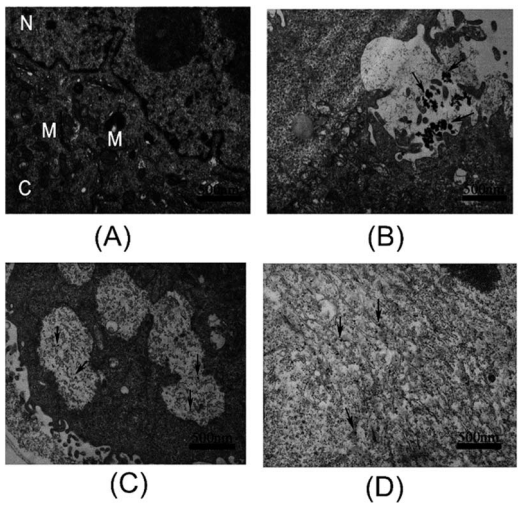

Fig. 4 TEM image of TiO_2 nanoparticle internalization in HeLa cells. (A) Control group of normal HeLa cells. The nucleus is denoted N, the mitochondria M and the cytosol C. (B) Caveolae-mediated endocytosis. (C) TiO_2 nanoparticles were found in the endosome. (D) Many TiO_2 nanoparticles were found freely dispersed in the cytosol. The arrows indicate the TiO_2 nanoparticles. Scale bars are 500 nm.

endosomes and were surrounded by a membrane suggesting that they were taken into the endosomes from the outside of the cell by caveolae. Interestingly, many TiO_2 nanoparticles do not aggregate in the endosomes, but are found freely dispersed in the cytosol (Fig. 4D) although the observed endosomal uptake mechanism remains clearly dominant. These findings indicate that TiO_2 nanoparticles are not only distributed in the endosomes but that they can also escape from the endosomes and distribute freely in the cytosol. The TEM image in Fig. 4D also shows that TiO_2 nanoparticles are distributed in the cytoplasm of HeLa cells but we did not observe nanoparticles in the cell nucleus.

To further validate the intracellular distribution of TiO_2 nanoparticles, we attempted to analyze TiO_2 nanoparticles exposed to HeLa cells with TXM. As shown in Fig. 5A, the transmitted image of normal HeLa cells was obtained by TXM

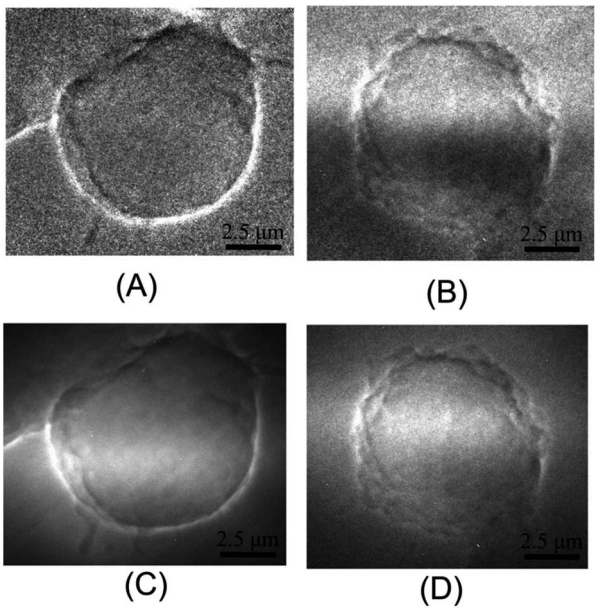

Fig. 5 X-ray microscope image of TiO_2 nanoparticle internalization in HeLa cells. (A) Transmitted image of normal HeLa cells (control). (B) The transmitted image of TiO_2 nanoparticle (100 μg ml^{-1}) internalization in HeLa cells. (C) Scanning image of normal HeLa cells (control). (D) Scanning image of TiO_2 nanoparticle (100 μg ml^{-1}) internalization in HeLa cells. Scale bars are 2.5 μm.

and the cell membrane as well as the cell profile are clear. However, the subcellular structures such as the cell nucleus and mitochondria cannot be clearly imaged. When 100 μg ml^{-1} of TiO_2 nanoparticles were exposed to the cells for 24 h, the transmitted image of the cells show that the cell surface was very rough (Fig. 5B). This is probably caused by the cytotoxicity of the TiO_2 nanoparticles. The images scanned using TXM were consistent with the transmitted images (Fig. 5C and D). These results demonstrate that subtle changes in the cellular surface morphology can be easily detected by TXM.

As shown in the 3D reconstructed tomography images in Fig. 6A and B, most of the TiO_2 nanoparticle aggregates are distributed over the cell membrane surface (movie provided as ESI†: Fig. 7B mpg). However, the TiO_2 nanoparticle distribution

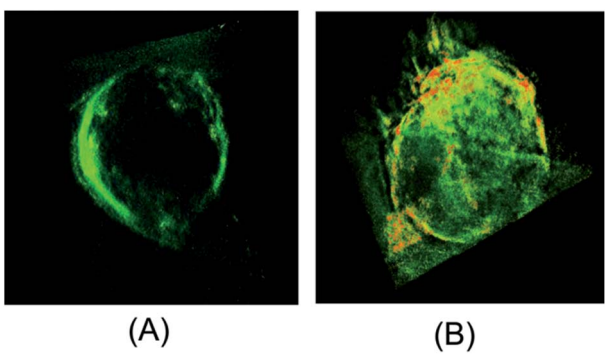

Fig. 6 3-D representation of the X-ray microscope image for TiO_2 nanoparticle internalization in HeLa cells. (A) 3-D image of a normal HeLa cell (control). (B) 3-D image of TiO_2 nanoparticle (red) distributions in the cell membrane.

in the cytosol could not be detected because of the resolution limitation. The resolution of TXM is not sufficient to resolve single nanoparticles as in TEM and only aggregates in the endosomes can be imaged. The possibility of tomographic reconstruction complements TEM. With the full 3D capability of TXM, we can definitively conclude that the nanoparticles are not present in the nucleus. Our experiment obtained a 3D cellular distribution of TiO_2 nanoparticle aggregate information at a resolution better than 100 nm using hard X-ray tomography. Although the results may not be very impressive compared with results from other well-developed techniques such as TEM, they demonstrate that hard X-ray tomography has the ability to examine the cellular distribution of nanoparticle aggregates and it can be used as a complementary analytical method to image the cellular distribution of nanoparticle aggregates.

Conclusions

We present a systematic study of cellular uptake and intracellular distribution of TiO_2 nanoparticles by transmission electron microscopy (TEM) and transmission X-ray microscopy (TXM). We found that TiO_2 nanoparticles are easily taken up by cells through endosomal routes. Within the cells, the majority of TiO_2 nanoparticles are found in the endosome, but the TiO_2 nanoparticles were also observed freely dispersed in the cytosol. Like many initial studies aiming to gain a simple insight into complex phenomena, this study raises more questions than it answers. For example, the nanoparticle uptake mechanism is not yet clear. Further studies are needed to explain the uptake mechanism and the intracellular fate of nanoparticles.

Acknowledgements

This work was supported by the Ministry of Science and Technology of China (2012CB825805, 2012CB932600), the National Natural Science Foundation of China (Nos. 11179004, 11275251, U1232113, U1232114, 31170077), the K.C. Wong Education Foundation and the Youth Innovation Promotion Association CAS.

Notes and references

1 M. Horie, H. Kato, K. Fujita, S. Endoh and H. Iwahashi, *Chem. Res. Toxicol.*, 2012, **25**, 605–619.
2 A. Z. Wang, R. Langer and O. C. Farokhzad, *Annu. Rev. Med.*, 2012, **63**, 185–198.
3 S. Parveen, R. Misra and S. K. Sahoo, *J. Nanomed. Nanotechnol.*, 2012, **8**, 147–166.
4 J. L. Chen and W. E. Fayerweather, *J. Occup. Med.*, 1988, **30**, 937–942.
5 I. Řehoř, V. Vilímová, P. Jendelová, V. Kubíček, D. Jirák, V. Herynek, M. Kapcalová, J. Kotek, J. Černý, P. Hermann and I. Lukeš, *J. Med. Chem.*, 2011, **54**, 5185–5194.
6 A. P. Zhang and Y. P. Sun, *World J. Gastroenterol.*, 2004, **10**, 3191–3193.
7 Y. Nakagawa, S. Wakuri, K. Sakamoto and N. Tanaka, *Mutat. Res.*, 1997, **394**, 125–132.
8 Q. Rahman, M. Lohani, E. Dopp, H. Pemsel, L. Jonas, D. G. Weiss and D. Schiffmann, *Environ. Health Perspect.*, 2002, **110**, 797–800.
9 J. J. Wang, B. J. S. Sanderson and H. Wang, *Mutat. Res., Genet. Toxicol. Environ. Mutagen.*, 2007, **628**, 99–106.
10 C. Y. Jin, B. S. Zhu, X. F. Wang and Q. H. Lu, *Chem. Res. Toxicol.*, 2008, **21**, 1871–1877.
11 J.-R. Gurr, A. S. S. Wang, C.-H. Chen and K.-Y. Jan, *Toxicology*, 2005, **213**, 66–73.
12 J. Chen, X. Dong, J. Zhao and G. Tang, *J. Appl. Toxicol.*, 2009, **29**, 330–337.
13 H. Liu, L. Ma, J. Zhao, J. Liu, J. Yan, J. Ruan and F. Hong, *Biol. Trace Elem. Res.*, 2009, **129**, 170–180.
14 E. Fabian, R. Landsiedel, L. Ma-Hock, K. Wiench, W. Wohlleben and B. van Ravenzwaay, *Arch. Toxicol.*, 2008, **82**, 151–157.
15 G. Schneider, *Ultramicroscopy*, 1998, **75**, 85–104.
16 T. Zheng, W. Li, Y. Guan, X. Song, Y. Xiong, G. Liu and Y. Tian, *Microsc. Res. Tech.*, 2012, **75**, 662–666.
17 W. W. Gu, L. D. Etkin, M. A. Le Gros and C. A. Larabell, *Differentiation*, 2007, **75**, 529–535.
18 G. McDermott, M. A. Le Gros, C. G. Knoechel, M. Uchida and C. A. Larabell, *Trends Cell Biol.*, 2009, **19**, 587–595.
19 D. Attwood, W. Chao, E. Anderson, J. A. Liddle, B. Harteneck, P. Fischer, G. Schneider, M. Le Gros and C. Larabell, *J. Biomed. Nanotechnol.*, 2006, **2**, 75–78.
20 C. A. Larabell and K. A. Nugent, *Curr. Opin. Struct. Biol.*, 2010, **20**, 623–631.
21 J. C. Andrews, F. Meirer, Y. J. Liu, Z. Mester and P. Pianetta, *Microsc. Res. Tech.*, 2011, **74**, 671–681.
22 (*a*) Y. S. Chu, J. M. Yi, F. De Carlo, Q. Shen, W. K. Lee, H. J. Wu, C. L. Wang, J. Y. Wang, C. J. Liu, C. H. Wang, S. R. Wu, C. C. Chien, Y. Hwu, A. Tkachuk, W. Yun, M. Feser, K. S. Liang, C. S. Yang, J. H. Je and G. Margaritondo, *Appl. Phys. Lett.*, 2008, **92**, 103119; (*b*) P. Cloetens, R. Mache, M. Schlenker and S. Lerbs-Mache, *Proc. Natl. Acad. Sci. U. S. A.*, 2006, **103**, 14626–14630.
23 J. Yi, Y. S. Chu, Y. T. Chen, T. Y. Chen, Y. Hwu and G. Margaritondo, *J. Phys. D: Appl. Phys.*, 2011, **44**, 232001.
24 G.-C. Yin, Y.-F. Song, M.-T. Tang, F.-R. Chen, K. S. Liang, F. W. Duewer, M. Feser, W. Yun and H.-P. D. Shieh, *Appl. Phys. Lett.*, 2006, **89**, 221122–221123.
25 T. Y. Chen, Y. T. Chen, C. L. Wang, I. M. Kempson, W. K. Lee, Y. S. Chu, Y. Hwu and G. Margaritondo, *Opt. Express*, 2011, **19**, 19919–19924.
26 B. J. Marsh, D. N. Mastronarde, K. F. Buttle, K. E. Howell and J. R. McIntosh, *Proc. Natl. Acad. Sci. U. S. A.*, 2001, **98**, 2399–2406.
27 O. Medalia, I. Weber, A. S. Frangakis, D. Nicastro, G. Gerisch and W. Baumeister, *Science*, 2002, **298**, 1209–1213.
28 D. Nicastro, A. S. Frangakis, D. Typke and W. Baumeister, *J. Struct. Biol.*, 2000, **129**, 48–56.
29 C. A. Larabell and M. A. Le Gros, *Mol. Biol. Cell*, 2004, **15**, 957–962.

30 G. Schneider, E. Anderson, S. Vogt, C. Knochel, D. Weiss, M. Legros and C. Larabell, *Surf. Rev. Lett.*, 2002, **9**, 177–183.
31 D. Weiss, G. Schneider, B. Niemann, P. Cuttmann, D. Rudolph and G. Schmahl, *Ultramicroscopy*, 2000, **84**, 185–197.
32 G. McDermott, D. M. Fox, L. Epperly, M. Wetzler, A. E. Barron, M. A. Le Gros and C. A. Larabell, *BioEssays*, 2012, **34**, 320–327.
33 D. Y. Parkinson, G. McDermott, L. D. Etkin, M. A. Le Gros and C. A. Larabell, *J. Struct. Biol.*, 2008, **162**, 380–386.
34 D. Parkinson, L. Epperly, G. McDermott, M. Gros, R. Boudreau and C. Larabell, in *Nanoimaging*, ed. A. A. Sousa and M. J. Kruhlak, Humana Press, 2013, vol. 950, pp. 457–481.
35 H.-H. Chen, C.-C. Chien, C. Petibois, C.-L. Wang, Y. Chu, S.-F. Lai, T.-E. Hua, Y.-Y. Chen, X. Cai, I. Kempson, Y. Hwu and G. Margaritondo, *J. Nanobiotechnol.*, 2011, **9**, 14.
36 X. Q. Cai, H. H. Chen, C. L. Wang, S. T. Chen, S. F. Lai, C. C. Chien, Y. Y. Chen, I. M. Kempson, Y. Hwu, C. S. Yang and G. Margaritondo, *Anal. Bioanal. Chem.*, 2011, **401**, 809–816.
37 X. Q. Cai, C. L. Wang, H. H. Chen, C. C. Chien, S. F. Lai, Y. Y. Chen, T. E. Hua, I. M. Kempson, Y. Hwu, C. S. Yang and G. Margaritondo, *Nanotechnology*, 2010, **21**, 335604.
38 J. Rauch, W. Kolch, S. Laurent and M. Mahmoudi, *Chem. Rev.*, 2013, **113**, 3391–3406.
39 L. Pelkmans, T. Burli, M. Zerial and A. Helenius, *Cell*, 2004, **118**, 767–780.

